Performance tests for mammographic film-screen combinations: use of absolute techniques

Doğan Bor, Kerime Akdur

PURPOSE

A performance comparison of film-screen combination used in mammography was conducted using conventional and new techniques.

MATERIALS AND METHODS

The performance of 30 mammographic film-screen combinations was evaluated by sensitometry, and the total performance was determined using phantom measurements. Quantum detection and light emission efficiency of the screens were also measured as an alternative technique for determining screen speeds. These efficiency measurements provided quantitative results for selecting the optimum beam quality.

RESULTS

Considering the image quality scores from three observers and the radiation doses obtained from the speed measurements, eight combinations were selected as being optimal. Only three of the mammographic film screen combinations in this group were the recommendations of manufacturers.

CONCLUSION

The total performance phantom can be effectively used for the qualitative check of image and provide speed information for mammographic film-screen combinations comparable to sensitometric techniques.

Department of Engineering Physics (D.B. ✉ bor@eng.ankara.edu.tr), Ankara University, Ankara, Turkey.

There are many studies in the literature comparing mammographic film-screen (F-S) combinations. These comparisons have been primarily for F-S sensitometry in some publications but have extended to other techniques aiming the evaluation of images obtained from breast simulating phantoms and also patient studies (1–11).

The replacement of analog systems with digital detectors during the last few decades has caused a dramatic drop in the F-S market. Finding new products is difficult, and manufacturers have stopped producing some of their former products. However, there are still many departments using analog systems and attempting to select the optimal F-S combinations. However, due to this limitation in production, some users have been faced with the challenge of finding the most suitable combination for their existing films or screens because the recommended combination is no longer available.

A considerable number of departments still use F-S combinations without following the manufacturer recommendations or use random combinations without any supporting experimental data. It should be kept in mind that, the determination of the F-S speeds through X-ray sensitometry and assessment of image quality using specific phantoms require skilled users.

Breast dose and image quality are the most important parameters to be optimized in mammographic examinations.

The X-ray sensitometry mainly gives the relative speed of the combination and some information about the contrast. A detailed investigation of image quality in terms of high- and low-contrast resolution, detection of abnormalities, and assessment of the breast doses requires the use of specific phantoms (12).

This work aimed to find optimal F-S combinations using five films paired with six screens using image quality and speed measurements. The utility of a total performance phantom was investigated due to its simple use. Three observers checked the image qualities by using the phantom images. Sensitometric tests were also used as alternative performance measurements of the F-S combinations. Because the screen speeds are mainly determined by their quantum detection and light emission efficiencies, they were measured using the cadmium telluride (CdTe) semiconductor detector and a photometer, respectively. The results of these measurements were used for selecting the optimal beam quality and also provided an absolute way for assessing screen speeds.

Materials and methods

All of the measurements were performed with a conventional mammographic unit (General Electric Alpha RT, GE Healthcare, Milwaukee,

Wisconsin, USA). The performance of this system was tested during the commissioning stage using the appropriate protocols (13, 14).

Film and screens were selected according to the results of a previous survey study reporting the types of F-S combinations used in many radiology departments (15). Thirty combinations of five different films with six different types of screens were selected for this study (Table 1).

Screen efficiency measurements

The quantum detection and light output efficiencies of each screen were determined at different beam qualities, and an optimal kVp was selected from these results.

The quantum detection efficiency of the screens was measured to determine the percentage of X-rays absorbed and to determine the most effective kVp. A 1 mm thick CdTe X-ray detector XR-100T (Amptek Inc., Bedford, Massachusetts, USA) with a 25 mm² active area was used to measure the screen quantum detection efficiencies (16). This detector was positioned 30 cm away from the focal spot and collimated with two tungsten collimators with 200 and 1000 μm diameters (Fig. 1). This collimation provided narrow beam geometry, and scatter-free data acquisition became possible. The detector output was sent to a multichannel analyzer (PX 5, Amptek Inc.) for spectrum measurement. The energy resolution of this detector at 122 keV (Co-57) is less than 1.5 keV, enabling the inspection of the incoming and transmitted X-ray spectra.

Each screen was positioned with the emulsion side facing to the X-ray tube at a distance of 8 cm. The exposures were made at seven different kVp (26–32) at 100 mAs but were repeated five times to ensure the statistical reliability. The ratios of the spectrum counts without screens (I_0) and with screens (I) were calculated and reported as the quantum detection efficiency (I_{QDE}).

$$I_{QDE} = (I_0 - I) / I$$

Although discriminating all of the peaks of the X-ray spectrum of the molybdenum (Mo) target due to the high resolution of the CdTe detector was possible, the total counts under

Table 1. Films and screens used in this work and their abbreviations	
Films	Abbreviation
Kodak MIN-R 2000	F1
Kodak MIN-R EV	F2
Kodak MIN-R S	F3
Agfa Mamoray HDR-C	F4
Retina XMA	F5
Screens	
Kodak MIN-R 2 EV 190	S1
Kodak MIN-R 2 MIN-R 2000	S2
Kodak MIN-R 2 MIN-R	S3
Kodak MIN-R 2 MIN-R 2190	S4
Agfa Mamoray HD S	S5
Cawo Mammo R 300	S6
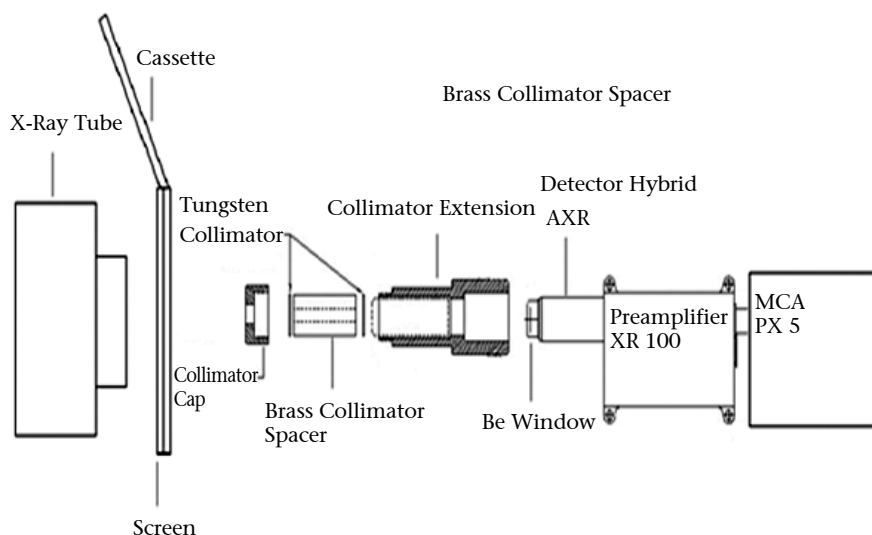
Figure 1. Schematic diagram of spectrum acquisition using cadmium telluride detector.

the whole spectrum were used for the statistical reliability of the results. The optimal operating kVp value for all of the screens was found in this way.

The light output efficiency of the screens was measured to see the quantity of the light emitted by the screen. A photometer (Precision Photometer 07-621, Fluke Biomedical, Cleveland, Ohio, USA) for these measurements was used according to the manufacturer's specifications, and its spectral response closely matched that of the *Commission Internationale de l'Éclairage* (CIE) photoptic response curve.

The experimental setup is given in Fig. 2. A screen was positioned 8 cm

away from the focal spot with a 25° angle with the emulsion side facing to tube. The exposures were made at 26, 27, 28, 29, 30, 31, and 32 kVp using 150 mAs in total room darkness. The photometer readings were recorded using the video format of a digital camera.

Sensitometric measurements

All of the films were processed using an automatic film processor (Protec Optimax 2010, Protec Processor Technology, Oberstenfeld, Germany) film processor with a 33°C developer temperature and a nominal processing time of 90 s with Kodak RP X-omat chemistry (Eastman Kodak Company, Roch-
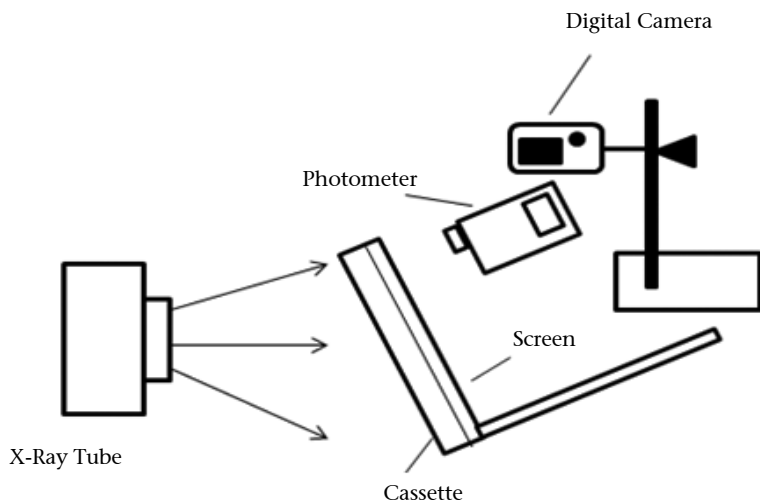
Figure 2. Experimental setup for measuring the screen light emission.

ester, New York, USA). Daily quality control of the processor was generated using a light sensitometer (Hand-Held Dual Color Electronic Sensitometer 07-417, Fluke Biomedical) and an optical densitometer (Hand-Held Deluxe Digital Clamshell Densitometer 07-443, Fluke Biomedical). The processor performance was stable enough to use for all of the experiments.

Light sensitometry

Light sensitometry analysis was performed for all of the films to test the performance of the film alone, and the film parameters, such as the average gradient and film speed, were determined using Hurter-Driffield (HD) curves.

X-ray sensitometry

The characteristic curves of 30 F-S combinations were obtained with the time scale and step wedge techniques. All of the exposures were performed at 28 kVp, which was decided based on the spectrum measurements using the Mo/Mo target filter combination, with a large focal spot (0.3 mm nominal size) and a 60 cm focus to film distance without the breast compression paddle.

In the time scale technique, the F-S cassette was loaded into the cassette holder, and a lead plate with a slit 3 cm wide was placed over the holder perpendicular to the anode-cathode axis. This lead plate was moved over the cassette holder after each exposure allowing for irradiation of the unexposed part of

the film. A total of 10 exposures were made by doubling the mAs each time within the range of 4–256 mAs, and 10 different gray levels were obtained on the film after processing. The optical densities were read, and the characteristic curves were plotted. Because the exposure was two times higher than the previous one, the exposure scale used in these plots was similar to those used in the plots of HD curves. To prevent the effect of time reciprocity low failure, extreme exposure times were not used. Similar to light sensitometry, the speed and average gradient of each combination were calculated.

Characteristic curves of the film screen combination were also obtained by exposing an aluminum step wedge with 15 steps and 9.5 cm in length. The wedge was positioned on the cassette holder with its long axis perpendicular to the anode-cathode axis to reduce the heel effect. The thickness of the step was 0.3 cm at the first step and gradually increased with a thickness of 0.39 cm (range, 0.26–0.49 cm) and reached a maximum thickness of 5.87 cm. An F-S combination of moderate speed (F1-S4) was selected as a reference and exposed at 28 kVp. The mAs of this exposure was adjusted until an optical density of approximately 1.8 was obtained on the film corresponding to the middle step of the wedge. This mAs value was then used for the exposures for the other combinations.

To compare the characteristic curves on a common exposure scale, a spec-

trum program (IPEM Report 78 Spectrum Processor©) was used. An X-ray spectrum similar to the one given by the mammography system was simulated with this software. The number of transmitted photons for each step was found using this program, and logarithms of transmission ratios for each step were used in the exposure scale for the characteristic curves. The speed and average gradient were again calculated for each combination.

Total performance phantom measurements

A commercially available phantom (CIRS Model 11A breast phantom, Norfolk, Virginia, USA) was used for testing the F-S combinations. Embedded patterns and structures in this phantom enable the users to make contrast and spatial resolution measurements for the F-S combinations.

This phantom, which included a 0.5 cm adipose-equivalent tissue layer, matches the composition of a 4.5 cm breast consisting of 50% glandular tissue and 50% adipose tissue, and is realistically shaped. Two line-pair test targets (5–20 lp/mm) with one parallel and one perpendicular to the anode-cathode axis, 13 groups of simulated microcalcifications, five different size nylon fibers simulating fibrous structure, seven different size tumor-like masses, a tissue equivalent step wedge consisting of five steps and an optical density reference zone were placed in this phantom.

The phantom was exposed at 28 kVp with different mAs (between six or nine settings) for each combination, but the selection of three mAs settings was done until the optical densities in the reference zone remained within the density ranges of 0.45–0.65 optical density (OD), 1.2–1.4 OD, and 2.20–2.7 OD. The images with medium density were used for all of the evaluations, but the images in the lower and higher density ranges were only used for some image quality comparisons considering the nonoptimal selection of exposure parameters.

Characteristic curves and entrance surface air kerma measurements

Using the films exposed to different mAs values, the optical densities were

read from the reference zone in the phantom image of each film. Characteristic curves (optical densities vs. mAs) were plotted for each combination, and the relative speeds were calculated from the mAs values (instead of logE) corresponding to the optical density of (Base+Fog)+1.0 OD.

The exposures were repeated using similar parameters without the phantom in the beam, and readings were taken by a suitable ion chamber AC-CU-PRO (Radcal Corporation, Monrovia, California, USA). Entrance surface air kerma (ESAK) values were determined from these readings after distance corrections were performed.

Contrast index measurements

Five different gray scales on the processed film were produced from the embedded step wedge built in the phantom. The optical density measurements from the gray scale were plotted against their step number, and the slope of this curve was defined as the contrast index and was compared with the average gradient of the characteristic curves obtained from the film sensitometry results.

Low contrast and spatial resolution measurements

Three independent observers scored a total of 90 images obtained at three optical density ranges for each combination. As a measure of low contrast, the number of visible embedded masses and fibers were counted, and as a measure of high-contrast spatial resolution, the number of discernible microcalcifications and line-pairs/mm were counted.

Results

Quantum detection efficiency and light output results

The quantum detection efficiencies of the screen have been determined for different beam qualities by acquiring the transmitted X-rays from the screen with a CdTe detector. In general, all of the screens showed a gradual increase in spectrum counts with the kVp due to a higher penetration of the beam in the screen. There were some fluctuations in the response of some screens with the kVp, most likely due to the

escape of characteristic X-rays and the K-absorption edge of the screen materials. Twenty-eight kVp was found to be the most adequate kVp for all of the screens because the responses of screens in this setting were free from these fluctuations. Although the detection efficiencies of S2, S3, S5, and S4 were quite close to each other, the efficiency of the S6 and S1 screens was higher than the others (Fig. 3).

Similar to the determination of quantum detection efficiencies, the light output efficiencies of the screens were also measured at different beam qualities, and with the exception of some small fluctuation noticed in some screens, a higher output was also noticed for the S6 and S1 screens (Fig. 4).

Both efficiencies are important for screen speed, but the intensity of the light emitted from the screen and its match with the film (not measured in this work) seems to be more important. For example, S3 was found to be the slowest in the sensitometry results, and although S3 had a higher quantum efficiency than the others, its light emission was the weakest, thus confirming its low speed.

Light and X-ray sensitometry

Fig. 5 shows the HD curves of five films obtained with light sensitometry. In Figs. 6 and 7, the characteristic curves for the F1 film, with all of the screens for the time scales and step wedges, are shown. The curves for the other combinations are not included in the text, but the speeds and average gradients of 30 combinations have been calculated from these plots.

These evaluations addressed two aims. One was to find the most adequate screen for a specific film, and the second was to identify the optimum film for an existing screen. During these evaluations, a comparison of the two sensitometric techniques was also performed.

To find the best screen for the films selected for this study, the maximum speed of each film when exposed separately to each screen was found for the two techniques. Table 2 indicates the maximum speeds obtained for each film when exposed to each screen combination. The S6 screen was found to be the fastest screen when exposed to each film. This result indicates that the screens are mainly responsible for the F-S speed. Due to the limited space in
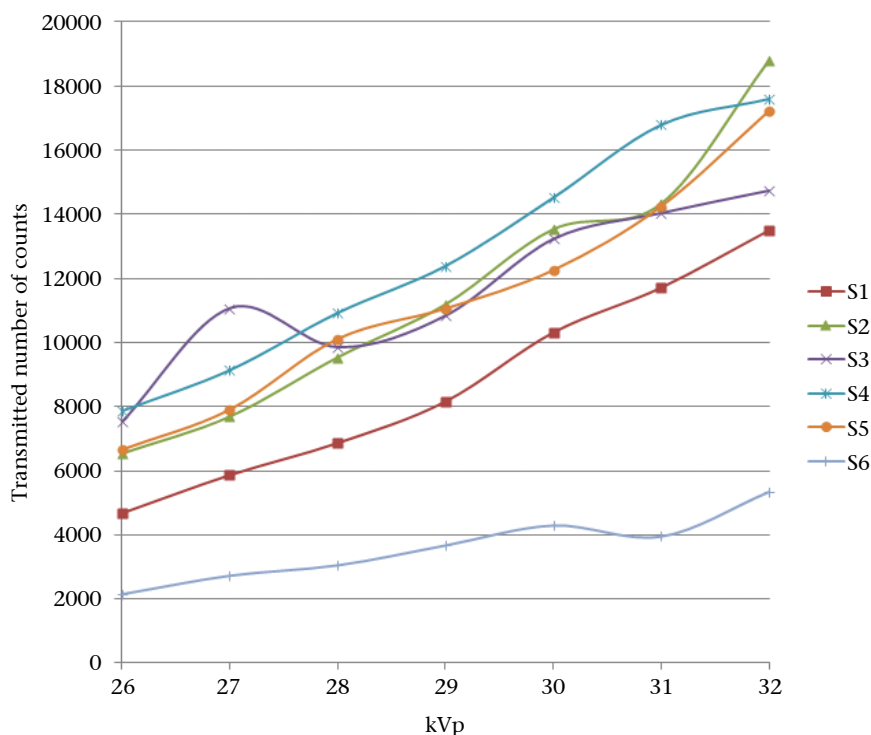
Figure 3. Quantum detection efficiencies of the screens (S) using different beam qualities.
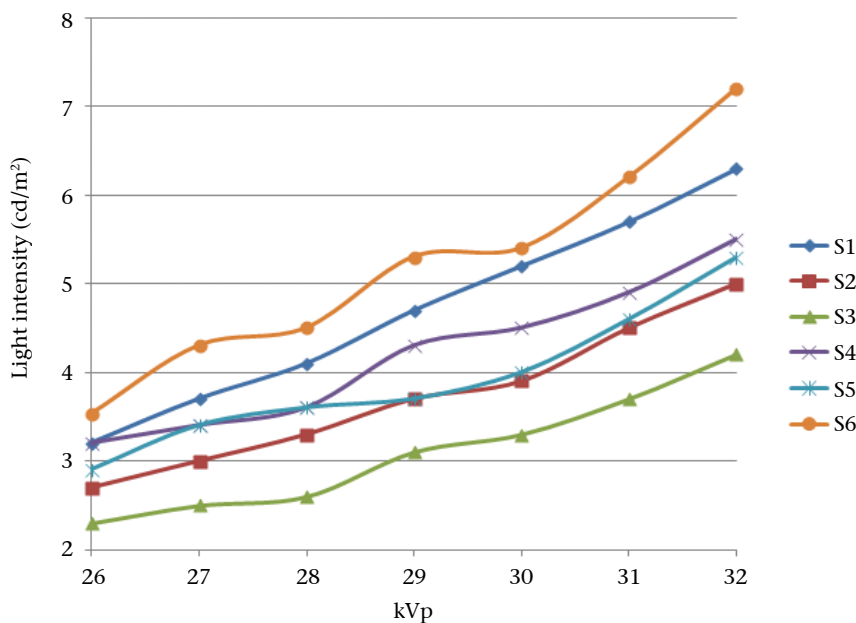
Figure 4. Light emission efficiencies for the screens (S).

Film	B+F	Speed	Contrast
F1	0.24	88	2.45
F2	0.26	81	3.34
F3	0.28	100	3.37
F4	0.24	91	2.28
F5	0.28	98	3.35
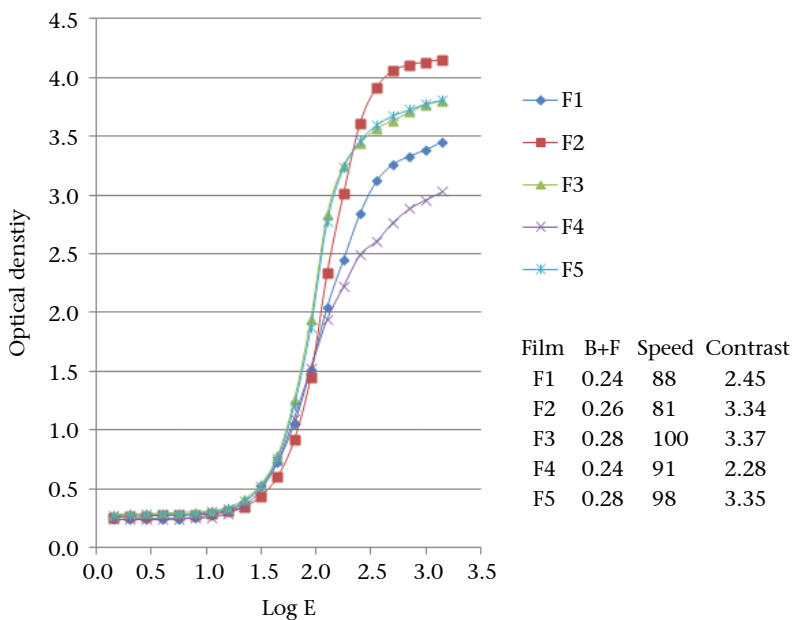
Figure 5. Hurter-Driffield curves for films (F) obtained using light sensitometry. The average gradients and speeds of each film are also indicated. B+F, Base+Fog.

the manuscript, only the screen with the maximum speed was included in the Table 2, and the order for the speed of the screens was similar for both techniques as follows: S6, S1, S4, S5, S2, and S3.

The sensitivity of each film to different screens can be better observed for the time scale technique in Table 2. The F5 and F3 films, which were the fastest films in the light sensitometry analysis, were found to be less sensitive than the others when used with different screens. Thus, screen selection for the slow film becomes more critical than for faster films according to the results using the time scale technique.

If another comparison was made among the films by taking the mean speeds of screen combination for each film, similar speed sequencing would be observed for each technique (F3, F5, F4, F1, and F2), which would also be similar to the light sensitometry speed ranking (Table 3).

If the average gradients are compared, the combinations giving maximum values show different screens for each film group (Table 4). This result confirms the fact that the contrast of the F-S combinations is mainly determined by the film contrast. The average gradient variations for each film when used with different screens are larger for the time scale technique.

The second aim was to find the optimal film for a specific screen. This aim was investigated by exposing each screen with each film using the two techniques. As indicated in Table 5, the F3 and F5 films yielded the fastest combinations, and the differences among the films for each screen were higher when using the time scale technique. The differences were larger for the slow screens (S3 and S2) for both techniques. Film selection for the slow screens is more critical; in other words, the slow screens are more sensitive when used in combination with different films. Similar to Table 2, only the films with the maximum speeds were included in the Table 5. The order for the speed of the films was similar for both techniques and was as follows: F3, F5, F1, F4, and F2.

The speed and contrast results for all of the combinations obtained from three techniques are shown in Table 6. Due to the differences in object contrast and exposure scales, comparisons were performed separately for each technique by taking the F1-S3 combination as a reference (100) for each comparison. As shown in the Table, the order for the fastest and slowest screens and the maximum and minimum contrast values have good correlations.

Total performance phantom

An alternative sensitometric measurement was also obtained from the exposure of the total performance phantom at different exposure levels for each F-S combination. In Fig. 8, the optical density versus the mAs graph is given for the F1 film exposed to oth-

er screens. The shape of these curves is quite similar to that observed when using the time scale and step wedge techniques, with the exception of the lower average gradients due to the scatter caused by the phantom thickness and construction. To calculate relative speed from these curves, the mAs (or exposure) values corresponding to (Base+Fog)+1.0 OD were determined.

Figure 6. Characteristic curves of F1 with different screens (S) obtained using X-ray sensitometry and the time scale method.

Table 2. Fastest screens for each film and speed differences for six screens when used with a specific film

	Time scale		Step wedge	
Film	Screen	Difference (%)	Screen	Difference (%)
F1[a]	S6	150	S6	120
F2	S6	179	S6	123
F3	S6	136	S6	139
F4	S6	187	S6	130
F5	S6	123	S6	132

[a]Example; when F1 was exposed separately to the S1 to S6 screens, the fastest combination was found for S6 and the speed difference between the combinations with F1 was 150%.

Table 3. Comparisons of the film groups

	Time scale		Step wedge	
Order of speed	Film	Average speed	Film	Average speed
1[a]	F3	333	F3	206
2	F5	314	F5	185
3	F1	301	F4	179
4	F4	257	F1	164
5	F2	249	F2	152

[a]Example; for F1, the mean of the speed for the six screens was 333. If these means are determined for each film group, then the film speeds can be compared.

The speed order for each film group was found to be quite similar for the three techniques (Table 6). The relative speeds are given in parentheses.

The contrast index values measured from the total performance phantom were normalized to the ESAK values and compared with the average gradients obtained from the characteristics curves. Although there are some small variations among the findings, comparable results were found using the other techniques (Table 6).

Evaluation of image quality

The measurement of low contrast detectability and high contrast spatial resolution is an additional advantage of using a total performance phantom. Table 7 shows the image quality results in terms of the number of microcalcifications, fibers and masses and line-pairs/mm for all of the combinations obtained in the mid-density range (1.2–1.4 OD). The contrast and resolution of the films were slightly different from each other in the mid-density range because the linear portions of their characteristic curves were very close to each other. In general, the F5 and F3 films gave better image quality when used with S1, S2, S4, and S5 screens. The poorest results were obtained with the fastest (S6) and slowest (S3) screens. Combinations with either F1 or F4 had the lowest image quality scores.

The image quality results obtained from the films with lower and higher optical densities are not given here, but the shape of the HD curve at the toe and especially at the shoulder region is expected to strongly affect these results. For example, the poor low contrast detectability of the F1 and F4 films can be well confirmed due to their early saturation.

Discussion

The speed of the screens is one of the main factors for the determination of the breast radiation dose; therefore, a correct assessment is necessary. The measurement of quantum detection and light yield efficiencies has provided an absolute way to determine their speed and their responses to different beam qualities.

Instead of acquiring sensitometric data and phantom images for each

Table 4. Average gradients for each film and speed differences for six screens when used with a specific film

	Time scale		Step wedge	
Film	Screen	Difference (%)	Screen	Difference (%)
F1[a]	S2	13	S2	4
F2	S4	13	S3	7
F3	S5	36	S3	3
F4	S5	25	S5	6
F5	S1	11	S2	3

[a]Example; maximum contrast for F1 was obtained with S2, and the difference of the other screens from this maximum was 13%.

Table 5. Fastest films for each screen and the speed differences for five films when used with a specific screen

	Time scale		Step wedge	
Film	Screen	Difference (%)	Screen	Difference (%)
S1[a]	F3	41	F5	20
S2	F3	47	F3	28
S3	F5	61	F3	18
S4	F5	43	F3	27
S5	F5	27	F3	27
S6	F5	30	F3	27

[a]Example; when S1 was exposed separately to the F1 to F5 films, the fastest combination was with F3, and the speed difference between the combinations of S1 was 41%.

Figure 7. Characteristic curves of F1 with different screens (S) obtained using X-ray sensitometry and the aluminum step wedge method.

beam quality, an optimum working voltage of 28 kVp with the Mo/Mo target-filter combination has been selected for all of the tests. This conclusion was also confirmed by other studies in the literature (17–19).

The optimal combinations of 30 F-S pairs were investigated in this work by sensitometry and total performance phantom and efficiency measurements. There are no well-established techniques for the F-S combination comparisons that could be easily implemented by the users. Manufacturers usually report their specifications using HD curves obtained with X-ray sensitometry. However, users generally have difficulty creating similar manufacturer setups. Moreover, these tests do not yield information regarding the clinical performance of the combinations, and each technique has its own limitations. The time scale is time consuming and requires a generator with excellent exposure reproducibility and reciprocity. Additionally, reciprocity low failure may affect the results. The aluminum step wedge technique is easy to implement, but scatter from the thick steps may reduce the accuracy of this method. When these two techniques were compared, similar shapes of the curves and speed sequences were observed, but the curves of different combinations were more discernible for the time scale technique. The effects of the different screens and also screens when exposed to each films and films on the speed and contrast of the combination were well understood from the responses of the films when exposed to each of the screens. The contrast of the combinations was determined with the film contrast, and this finding was confirmed by the light sensitometry results. The screens were mainly responsible for the speed of the combinations, and this conclusion is also supported by the results of the quantum detection and light efficiency measurements.

We believe that users can easily use the total performance phantom for comparing all of the F-S combinations. The relative speeds and contrasts among the combinations were found to have good agreement with the X-ray sensitometry techniques. Additional information regarding to the low contrast and spatial resolution can also be gained. Low and
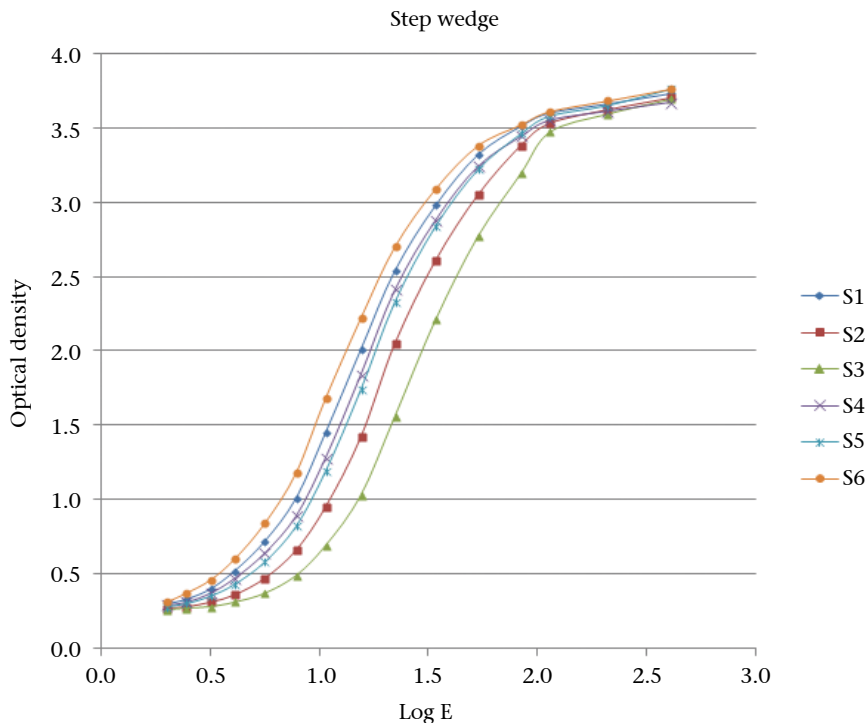
Table 6. Comparison of the speed and contrast for the three different techniques

Sequence no.	Time scale		Al step wedge		Total performance phantom	
	Speed	Contrast	Speed	Contrast	Speed	CI*100-ESAK
1	F5-S6 (292)	F3-S5 (4.29)	F3-S6 (268)	F5-S2 (3.91)	F1-S5 (293)	F5-S6 (4.83)
2	F3-S6 (285)	F3-S4 (3.65)	F5-S6 (254)	F5-S3 (3.88)	F5-S6 (241)	F3-S6 (4.69)
3	F1-S6 (250)	F5-S1 (3.53)	F4-S6 (223)	F5-S5 (3.86)	F3-S6 (241)	F3-S1 (3.99)
4	F3-S1 (247)	F5-S5 (3.52)	F1-S6 (220)	F3-S3 (3.86)	F3-S1 (216)	F3-S4 (3.90)
5	F4-S6 (246)	F3-S2 (3.49)	F5-S1 (216)	F3-S2 (3.85)	F3-S4 (205)	F5-S1 (3.88)
6	F1-S1 (239)	F5-S2 (3.41)	F3-S1 (212)	F5-S4 (3.83)	F5-S1 (205)	F5-S4 (3.85)
7	F2-S6 (224)	F3-S1 (3.38)	F2-S6 (208)	F5-S1 (3.82)	F2-S6 (205)	F3-S5 (3.43)
8	F5-S4 (218)	F5-S4 (3.25)	F3-S4 (200)	F5-S6 (3.80)	F1-S6 (205)	F2-S6 (3.37)
9	F3-S5 (173)	F5-S6 (3.23)	F1-S1 (194)	F3-S1 (3.78)	F1-S1 (195)	F5-S5 (3.22)
10	F3-S4 (206)	F3-S3 (3.22)	F4-S1 (194)	F3-S5 (3.78)	F5-S4 (186)	F3-S2 (3.07)
11	F5-S5 (187)	F2-S4 (3.19)	F5-S4 (193)	F3-S6 (3.78)	F4-S6 (186)	F2-S4 (3.01)
12	F1-S5 (185)	F5-S3 (3.17)	F3-S5 (191)	F2-S3 (3.77)	F3-S5 (178)	F5-S2 (2.99)
13	F1-S4 (184)	F2-S5 (3.16)	F5-S5 (183)	F2-S2 (3.76)	F4-S1 (171)	F2-S1 (2.96)
14	F5-S1 (244)	F3-S6 (3.15)	F2-S1 (181)	F3-S4 (3.75)	F5-S5 (171)	F1-S4 (2.81)
15	F2-S1 (182)	F2-S3 (3.10)	F1-S4 (173)	F2-S5 (3.68)	F2-S1 (171)	F1-S1 (2.37)
16	F4-S1 (175)	F2-S6 (3.09)	F4-S4 (171)	F2-S4 (3.63)	F1-S4 (171)	F5-S3 (2.25)
17	F3-S2 (170)	F2-S1 (2.96)	F1-S5 (162)	F2-S1 (3.60)	F4-S5 (158)	F3-S3 (2.25)
18	F2-S4 (165)	F2-S2 (2.83)	F4-S5 (159)	F2-S6 (3.50)	F4-S4 (158)	F4-S1 (2.25)
19	F4-S5 (165)	F4-S5 (2.70)	F2-S4 (157)	F4-S5 (2.82)	F2-S4 (158)	F2-S5 (2.24)
20	F5-S2 (159)	F4-S4 (2.60)	F3-S2 (153)	F4-S4 (2.79)	F3-S2 (146)	F4-S4 (2.23)
21	F2-S5 (159)	F4-S3 (2.54)	F5-S2 (152)	F4-S3 (2.74)	F2-S5 (141)	F4-S6 (2.22)
22	F1-S2 (158)	F4-S2 (2.46)	F2-S5 (150)	F4-S2 (2.73)	F5-S2 (137)	F1-S6 (2.22)
23	F4-S4 (152)	F4-S1 (2.46)	F1-S2 (133)	F1-S2 (2.73)	F1-S2 (128)	F2-S2 (2.16)
24	F4-S2 (131)	F1-S2 (2.46)	F4-S2 (130)	F4-S1(2.72)	F4-S2 (121)	F1-S2 (2.12)
25	F5-S3 (131)	F1-S3 (2.36)	F2-S2 (120)	F1-S3 (2.70)	F2-S2 (114)	F4-S5 (2.03)
26	F3-S3 (121)	F1-S4 (2.33)	F3-S3 (110)	F1-S5 (2.69)	F5-S3 (105)	F1-S5 (2.03)
27	F2-S2 (115)	F1-S6 (2.33)	F5-S3 (109)	F4-S6 (2.67)	F3-S3 (103)	F4-S2 (1.81)
28	F1-S3 (100)	F1-S5 (2.26)	F1-S3 (100)	F1-S1 (2.62)	F1-S3 (100)	F2-S3 (1.74)
29	F4-S3 (86)	F1-S1 (2.17)	F4-S3 (97)	F1-S4 (2.62)	F4-S3 (93)	F1-S3 (1.42)
30	F2-S3 (80)	F4-S6 (2.16)	F2-S3 (93)	F1-S6 (2.62)	F2-S3 (82)	F4-S3 (1.34)
Mean	181	2.95	177	3.34	166	2.76

Al, aluminium; CI, contrast index; ESAK, entrance surface air kerma; F, Film; S, Screen.

high optical density images can also provide useful information for the performance of F-S, if one wants to observe the effect of the wrong exposure settings and the effect of the shoulder and toe portions of the HD curves.

Finding papers in the literature comparing F-S combinations similar to those tested in this study is difficult. In one of the studies, the F5-S4 combination was found to be 1.12 times faster than F5-S2, which correlates with our finding that F5-S4 was 1.27 times faster than F5-S2 (7). As reported in the manufacturer data sheet, the average gradient of F2 was 1.26 times higher than F1, and its combination with S1 was found to be slightly faster than F1-S2; these findings correlated well with our results (20).

We also have some other results that agree with the manufacturer's reports. For example, the contrast values for F1 film with the S2, S3, and S4 screens were similar. This pattern was also true for the F3 film combinations (S2, S3, S4). In addition, the F3 combinations had higher contrasts than the F1 combinations, and their speed rankings were similar to our findings (i.e., F1-S4>F1-S2>F1-S3 and F3-S4>F3-S2>F3-S3) (20, 21).

Table 7. Image quality scores for the total performance phantom

Films	Screens	Calcium carbonate	Nylon fibers speck groups	75% glandular masses number	Line pair (Lp/mm) Perpendicular	Parallel
F1	S1	4.0	4.3	5.0	12.0	11.7
	S2	4.0	4.0	4.3	11.7	11.7
	S3	4.3	4.3	5.0	11.7	11.7
	S4	4.7	4.3	5.0	10.7	11.0
	S5	4.7	4.3	4.7	11.3	11.7
	S6	4.0	4.3	4.7	10.7	10.7
F2	S1	4.0	3.3	4.7	11.0	10.7
	S2	4.7	4.7	5.3	12.0	12.0
	S3	5.0	4.3	5.7	11.3	11.7
	S4	4.7	3.7	5.3	11.0	11.3
	S5	4.3	4.3	5.0	11.7	12.0
	S6	4.0	3.7	5.0	11.0	11.0
F3	S1	4.0	3.7	5.0	11.0	11.0
	S2	4.3	4.0	5.3	11.3	11.7
	S3	4.7	4.3	5.0	11.7	11.7
	S4	4.3	4.0	5.0	11.0	11.0
	S5	4.0	4.3	5.0	11.3	11.7
	S6	4.0	3.7	4.7	10.3	10.3
F4	S1	3.7	3.3	4.3	11.0	10.3
	S2	4.7	3.7	5.0	11.7	11.7
	S3	4.3	4.0	5.7	11.7	11.7
	S4	4.7	3.3	4.3	11.7	11.3
	S5	4.0	4.0	5.0	11.7	11.7
	S6	4.0	4.0	4.7	10.7	10.0
F5	S1	4.0	4.3	4.7	11.0	11.3
	S2	4.0	4.0	4.7	11.3	11.3
	S3	4.3	4.0	4.7	11.7	11.7
	S4	4.0	3.7	5.7	10.7	11.3
	S5	4.0	4.0	5.0	11.3	11.7
	S6	4.0	4.0	4.3	10.3	10.3

Selection of the best combinations

The speed, contrast and image quality scores were considered to be the main parameters for determining the optimal combinations. Considering the breast dose-image quality balance, combinations with high speed, high contrast and high image quality were the best, and those with low speed, low contrast and poor image quality were considered to be the worst combinations.

The best combinations were selected based on the information in Tables 6 and 7. Because the fastest combinations gave the poorest image quality and slowest combinations delivered the highest breast doses, an initial speed range (150–250) for the combinations was selected. The ESAK values equivalent to this range were 2.0–3.0 mGy/OD. In the second phase, the image quality scores from the total performance phantom for each combination were evaluated for each observer, and the average of their readings was calculated. The same logic was also applied to the average gradient results. Finally, those combinations with image quality scores and average gradients lower than the mean values together with those with speed values out of the acceptable range were eliminated. The eight selected combinations are presented as a contrast versus speed plot (Fig. 9).

Three out of eight combinations (F2-S1, F3-S2, F3-S4) were the pairs recommended by the manufacturers. However, some of the other recommended combinations (F1-S2, F1-S3, F1-S4, F3-S3 and F4-S5) failed in these evaluations (20–23).

The use of total performance phantoms or X-ray sensitometric tests enables users to select the best F-S combinations. However, many users cannot perform these tests, and they may request technical assistance. One of the most important results of this study was the determination of alternative combinations for different films and screens that are still used by many departments. Measurements of the quantum detection and light emission efficiencies of the screens to determine screen speeds confirmed the results of the phantom tests. Considering the essential role of screen speed for the breast radiation dose, these measures provide good results but require comprehensive instrumentation and user experience and therefore can only be
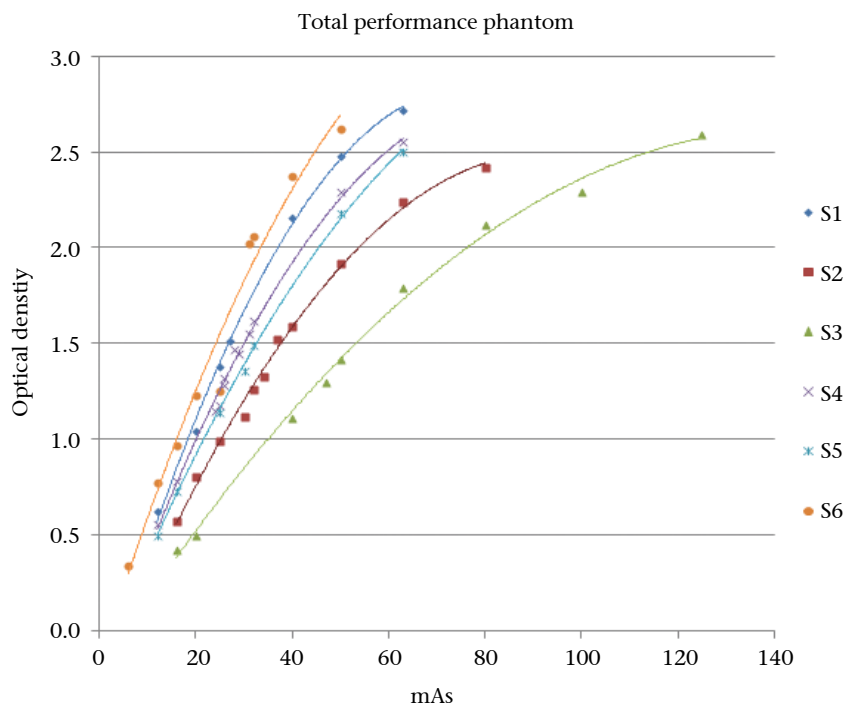
Figure 8. The optical density versus mAs graph is given for the F1 film exposed to other screens (S) during the total performance phantom exposure.
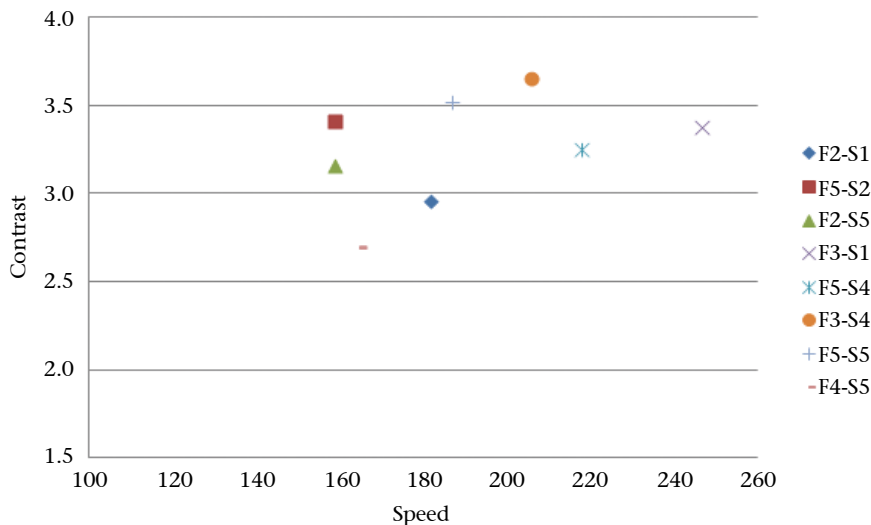
Figure 9. Selected film-screen combinations indicated in the contrast-speed diagram.

performed in well-equipped scientific laboratories.

In conclusion, the breast radiation dose and image quality in F-S mammography have always played a vital role in this modality and are strongly affected by the selection of the optimal F-S combination. A total performance phantom can be effectively used for comparing F-S combinations because the important parameters of the image quality and relative speeds can be obtained from one image. If the data regarding to the screen quantum detection and light emission efficiencies can be obtained once, this information can be used for the absolute values for the screen speeds and also for the optimal selection of beam quality. Together with film specifications, this information may help users to determine their optimal F-S combinations without necessitating comprehensive measurements.

Conflict of interest disclosure

The authors declared no conflicts of interest.

References

1. Haus AG, Rossmann K. X-ray sensitometer for screen-film combinations used in medical radiology. Radiology 1970; 94:673–678.
2. Fernández JM, Guibelalde E. Technical note: physical evaluation of recent Kodak films for mammography. Br J Radiol 1993; 66:828–832. **[CrossRef]**
3. Dimakopoulou AD, Tsalafoutas IA, Georgiou EK, Yakoumakis EN. Image quality and breast dose of 24 screen-film combinations for mammography. Br J Radiol 2006; 79:123–129. **[CrossRef]**
4. McParland BJ. A comparison of two mammography film-screen combinations designed for standard-cycle processing. Br J Radiol 1999; 72:73–75.
5. McParland BJ, Boyd MM, Yousef K AL. Optimizing optical density of a Kodak mammography film-screen combination with standard-cycle processing. Br J Radiol 1998; 71:950–953.
6. Kimme-Smith C, Basset LW, Gold RH, Zheutlin J, Gornbein JA. New mammography screen/film combinations: imaging characteristics and radiation dose. Am J Roentgenol 1990; 154:713–719. **[CrossRef]**
7. Tsalafoutas OA , Kolovos CA, Tsapaki V, et al. Evaluation of a new mammographic film: methods and considerations. Health Phys 2008; 94:338–344. **[CrossRef]**
8. Law J. Recent films and screens for mammography. Br J Radiol 1990; 63:966–967. **[CrossRef]**
9. Caldwell CB, Fishell EK, Jong RA, Weiser WJ, Yaffe MJ. Evaluation of mammographic image quality: pilot study comparing five methods. Am J Roentgenol 1992; 159:295–301. **[CrossRef]**
10. Qu G, Zhenxue J, Honeyman-Buck JC, Walker JK, Honeyman-Buck JC. Novel dual screen-dual film combination for mammography. Proc SPIE 1998; 3336:572–582. **[CrossRef]**
11. Meeson S, Young KC, Ramsdale ML, Wallis MG, Cooke J. Analysis of optical density and contrast in mammograms. Br J Radiol 1999; 72:670–677.
12. Young KC, Oduko J. Evaluation of the Kodak Min-R EV mammography film-screen system. NHSBSP Equipment Report 0401, Guildford, 2004.
13. Mammography Quality Control Manual. American College of Radiology, 1999.
14. European Guidelines for Quality Assurance in Breast Cancer Screening and Diagnosis, Fourth Edition. European Commission, Brussels, 2006.
15. Bor D, Akyol O, Olgar T. Performance measurements of mammographic systems. Radiat Prot Dosim 2008; 129:165–169. **[CrossRef]**

16. Matsumoto M, Yamamoto A, Honda I, Taniguchi A, Kanamori H. Direct measurement of mammographic x-ray spectra using a CdZnTe detector. Med Phys 2000; 27:1490–1502. [CrossRef]
17. Beaman SA, Lillicrap SC. Optimum x-ray spectra for mammography. Phys Med Biol 1982; 27:1209–1220. [CrossRef]
18. Feig SA. Mammography equipment: principles, features, selection. Radiol Clin North Am 1987; 25:897–911.
19. Jennings RJ, Eastgate RJ, Siedband MP, Ergun DL. Optimal x-ray spectra for screen-film mammography. Med Phys 1981; 8:629–639. [CrossRef]
20. Carestream Health, Kodak MIN-R 2000 film, Technical information data sheet 4316. Carestream Health Inc., 2009.
21. Carestream Health, Kodak MIN-R S film, Technical information data sheet 8906. Carestream Health Inc., 2008.
22. Carestream Health, Kodak MIN-R EV film, Technical information data sheet 4354. Eastman Kodak Company, 2010.
23. Agfa Healthcare, Mamoray™ HDR-C film, Technical information data sheet. Belgium, 2005.